RESEARCH ON THE CONTROL SYSTEM OF CHARGING DEVICE OF MINE ELECTRIC LOCOMOTIVE

L. ZHANG[1], Y.G. DONG[2], Z.B. LI[3*]

In order to reduce the failure rate of mine electric locomotive charger and improve the stability and safety of mine electric locomotive charger, this paper aims at the backward situation of charger structure and control of mine electric locomotive. It takes the zbcf-150/190-400 mine electric locomotive charger used in a mine of Huaibei Mining Group Co., Ltd as the research object. By improving the main circuit power unit structure and control unit, based on the analysis of the main circuit model and control strategy of the active front-end rectifier, the predictive current control is adopted for the charging device of the electric locomotive. The experimental results show that the feasibility and effectiveness of the control system, to achieve the safety and efficiency of the system, meet the requirements of the application field.

Keywords: Rectifier, electric locomotive, battery charger, predictive current Control

1. Introduction

The mining electric locomotive is used for long-term transportation of underground and its road surface. Its working principle is that the transmission device drives the wheel to rotate, so as to drive the train, so as to complete the transportation of coal, gangue, materials, equipment and personnel. At present, China is using a variety of mining electric locomotives, the total number of about 60000 [1-2]. Charger is the basis of normal use of electric locomotive, so it is of practical significance to study the structure and control of mine electric locomotive charger, reduce the failure rate of charger and improve the utilization rate.

In all the large coal mines of Anhui Huaibei Mining Group, the average number of mining electric locomotives is about 15. At present, there are 14 electric locomotives in a mine. There are two main circuit structures for chargers. The disadvantage of the rectifier is that it can only provide a DC power supply in the form of a fixed power supply. Second, thyristor phase-controlled rectifier is used to provide DC power supply [3-4]. Generally, thyristor phase-controlled

[1] Anhui College of Mining and Technology, Anhui, Huaibei, 235000, China
[2] Hebei Vocational University of Technology and Engineering, Hebei, Xingtai, 054000, China
[3] * Bozhou University, Anhui, Bozhou, 236800, China, E-mail: qinhuh298@163.com

rectifier and diode uncontrollable rectifier have basically the same advantages and disadvantages. The difference is that when the trigger angle of thyristor phase-controlled rectifier is greater than 900, it can feedback energy from the load power to the grid [5-8], and at the same time, it will introduce harmonics to the power grid, which has obvious disadvantages.

In this paper, the active front end AFE (active front end AFE) is used to overcome the shortcomings and limitations of the above two rectifiers [9-13], which can realize the advantages of bidirectional energy flow, high power factor, small harmonic component at input [14-20], and controllable DC output voltage. On the basis of voltage-oriented vector control (VOC) and predictive current control [21-22], the rectifier can automatically complete the complex charging program of constant current and constant voltage automatic conversion. Three charging methods with different performance are used, including current adjustment, over-current reset, shutdown and program automatic shutdown. After the actual trial operation, the charger can meet the requirements of battery charging, and the charging effect is good, which meets the requirements of green power, and the performance is stable and safe.

2. Battery structure

The battery is mainly composed of tubular positive plate, pasted negative plate, micro porous rubber separator, polypropylene battery covers and battery tank, electrolyte and special exhaust plug. The battery cover and battery tank are sealed by hot melt. The battery adopts bipolar pole structure, and each pole can bear the loop current independently. When a single battery is combined into a battery group, welding connection is adopted to prevent sparks and reduce contact resistance to ensure its safety and reliability. The exposed live part of battery pole and connecting line is covered with special insulating protective cover to prevent short circuit and spark caused by contact of metal foreign matters. There are small holes for measurement on the insulating protective sleeve. The special exhaust plug is used in the battery, which has good air permeability, so that the hydrogen is not easy to accumulate, prevent the battery from gas expansion and burst, and the electrolyte cannot splash out at the same time. When the average temperature of electrolyte is 30℃, the capacity of battery should be tested within 1-24 hours after charging. The electrolyte temperature should be kept between 22-34℃, and the ambient temperature must be kept within 15-35℃. If the electrolyte temperature is not at 30℃, the actual capacity (5-hour rate) should be converted according to Eq.1. If the electrolyte temperature is not at 30℃, the electrolyte density can be converted into the electrolyte density at 30℃ according to the decrease or increase of electrolyte density by 0.0007g/cm3 for every 1℃ increase or decrease of temperature. When the density of the electrolyte meets the

requirements and the temperature does not exceed 30℃, it can be added into the battery. The liquid level should be 20-25mm higher than the protection plate. After 4-6h of static state, the initial charging can be carried out according to the parameters.

$$C_{\alpha} = \frac{C}{1+0.006(t_0 - 30^0)} \tag{1}$$

where: C_{α}:actual capacity ah at - 30℃. C:- measured capacity ah.t_0: average temperature℃. 0.006: temperature coefficient.

3. Charger structure

The charger is connected to the insulation terminal board on the side of the transformer by the primary and secondary outlet terminals of the rectifier transformer. The primary tap is connected by △when the power supply voltage is 660V, and Y is connected at 1140V. Figure 1 shows the circuit diagram of the system. The main power is composed of flameproof switch, fast fuse rectifier transformer, varistor, PWM rectifier circuit and DC smoothing reactor. The function of varistor in the circuit is to protect the switching overvoltage and limit the surge current in the circuit. The fast fuse is used for the short circuit protection of the circuit. The wire across the two ends of the battery in the main circuit is reverse connection protection. When the charger is inversely connected with the battery pack, the battery pack's own voltage is connected to the coil of the main circuit reverse connected protection relay (the relay is installed in the reverse connection protector box), and the relay is closed to cut off the power supply of the control circuit of the starter in the main circuit. Then the power cannot be transmitted. At the same time, the sound and light alarm is given. The block diagram of the system structure is shown in Fig. 1.

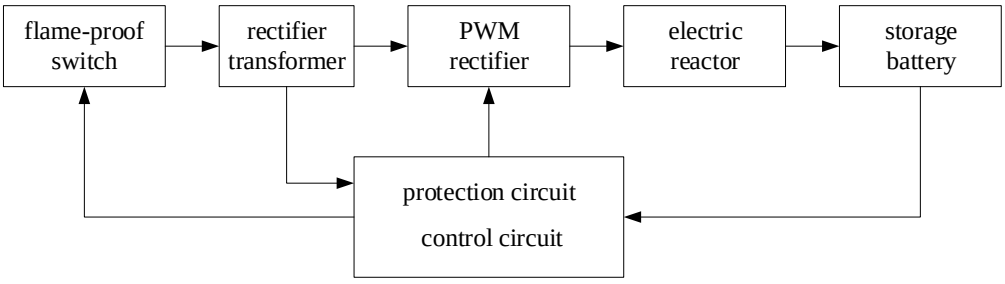

Fig. 1: Block diagram of the system structure

4. PWM rectifier model

Fig. 2 shows the active front-end rectifier model. The rectifier adopts a fully controlled bridge circuit composed of insulated gate bipolar transistor

(IGBT). The three-phase voltage source e_s (s = a, b, c) is connected by inductor L and resistance R. In the figure, e_a, e_b, and e_c are three-phase symmetrical AC power supply voltage, resistance R is resistance equivalent value of IGBT internal resistance and grid side filter inductance of three-phase switching device insulated gate bipolar transistor, and inductance L is equivalent value of external reactor and internal equivalent inductance of AC power supply [8]. Inductance L is the necessary condition to ensure the normal operation of PWM rectifier.

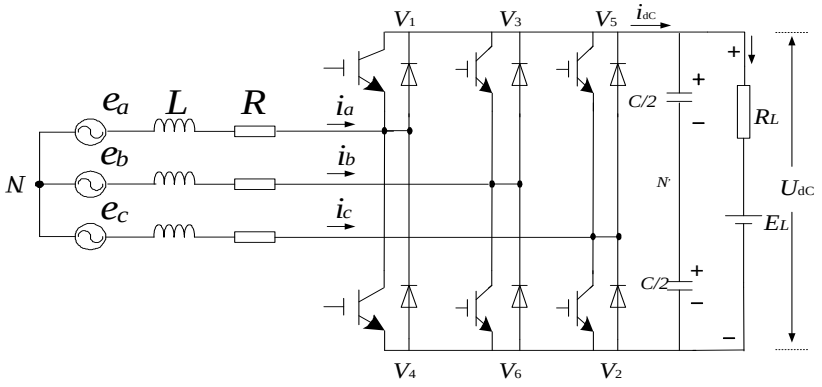

Fig.2: Three phase active front end rectifier

According to the circuit shown in Fig. 2, the equation of each phase can be expressed as Eq.2.

$$\begin{cases} e_a = L\dfrac{di_a}{dt} + Ri_a + u_{aN} - u_{nN} \\ e_b = L\dfrac{di_b}{dt} + Ri_b + u_{bN} - u_{nN} \\ e_c = L\dfrac{di_c}{dt} + Ri_c + u_{cN} - u_{nN} \end{cases} \tag{2}$$

Then, the space vector of grid voltage is defined as Eq.3.

$$u_s = \frac{2}{3}(e_a + ae_b + a^2 e_c) \tag{3}$$

where $a = e^{j\frac{2\pi}{3}}$. By substituting Eq.1 into Eq.2, the dynamic current vector equation for power grid can be obtained.

$$u_s = L\frac{d}{dt}(\frac{2}{3}(i_a + ai_b + a^2 i_c)) + R(\frac{2}{3}(e_a + ae_b + a^2 e_c)) + \frac{2}{3}(u_{aN} + au_{bN} + a^2 u_{cN}) - \frac{2}{3}(u_{nN} + au_{nN} + a^2 u_{nN}) \tag{4}$$

Eq.4 is equal to 0, which can be further obtained:

$$\frac{2}{3}(u_{aN}+au_{bN}+a^2u_{cN})=\frac{2}{3}(u_{nN}+au_{nN}+a^2u_{nN})=0 \tag{5}$$

Considering the following definitions of grid current vector and voltage vector generated by Active Frond End rectifier, the input dynamic current Eq.5 can be simplified as follows.

$$i_s=\frac{2}{3}(i_a+ai_b+a^2i_c) \tag{6}$$

$$u_{afe}=\frac{2}{3}(u_{aN}+au_{bN}+a^2u_{cN}) \tag{7}$$

The voltage u_{afe} is defined by the switching state of the converter and DC link voltage and can be expressed by the following Eq.8.

$$u_{afe}=S_{afe}U_{dc} \tag{8}$$

where U_{dc} is the DC side output voltage and S_{afe} is the PWM rectifier switching state vector. S_{afe} is determined by Eq.9.

$$S_{afe}=\frac{2}{3}(S_1+aS_2+a^2S_3) \tag{9}$$

where S_k,$(k=1,2,3)$ is the switching state of each bridge arm of PWM rectifier. If S_k=0, the bridge arm is the off state; if S_k=1, the bridge arm is the on state. Re input the dynamic current Eq.4 in the $\alpha\beta$ coordinate system to obtain the voltage Eq.10.

$$u_sL\frac{di_s}{dt}=u_s-u_{afe}-Ri_s \tag{10}$$

where i_s is the input current vector; u_s is the power line voltage; u_{afe} is the voltage generated by the converter.

5. Predictive current control

Predictive current control can generate several switching states based on static power converter. Predictive current control system model is used to predict the change characteristics of variables corresponding to each switching state. Therefore, before using predictive current control, the current selection criteria should be defined in advance. The purpose is to select the appropriate switching value that can be applied, such as the cost function. The main function of the cost function is to get the prediction of the variable parameter value to be controlled, and the error between the measured current and the reference current is minimized. The predictive current controller can calculate the predictive current by using a discrete-time model. The calculation formula is shown as Eq.11.

$$i_s(k+1) = (1-\frac{RT_s}{L})i_s(k) + \frac{T_s}{L}[u_s(k) - u_{afe}(k)] \tag{11}$$

For the sampling time Ts, this formula can be obtained by discretization through Eq.10, and the derivative term is approximated in one sampling period to realize the process of discretization. The predictive current controller can obtain the optimal current error with the minimum dynamic response speed. A more appropriate cost function can be selected to evaluate the input error value of the predictive current. The following mathematical expression is the cost function. In practical application, the absolute error between the predicted current and the reference current is taken into account and expressed in the form of rectangular coordinate system, as shown in Eq.12.

$$g = |i_{s\alpha}^{*} - i_{s\alpha}^{p}| + |i_{s\beta}^{*} - i_{s\beta}^{p}| \tag{12}$$

where $i_s(k+1) = i_{s\alpha}^{p} + ji_{s\beta}^{p}$ is the predicted value of input current at time $(k+1)$ for a given transformer, and the current $i_s^{*}(k) = i_{s\alpha}^{*} + ji_{s\beta}^{*}$ is the reference current value for time K.

6. Simulation and experiment

6.1 Simulation

Matlab/Simulink is used for simulation research. Simulation parameters: three phase symmetrical phase voltage 220V, equivalent resistance R=0.5Ω, inductance L=5mh, capacitance C=1500μf, voltage given as U_{DC}*=800V, switching to 600V in0.6s, R_L = 100 Ω, and R_L=50Ω in 0.3s. The simulation time is t_s =1 s. The simulation results are shown in Fig. 3- Fig. 6.

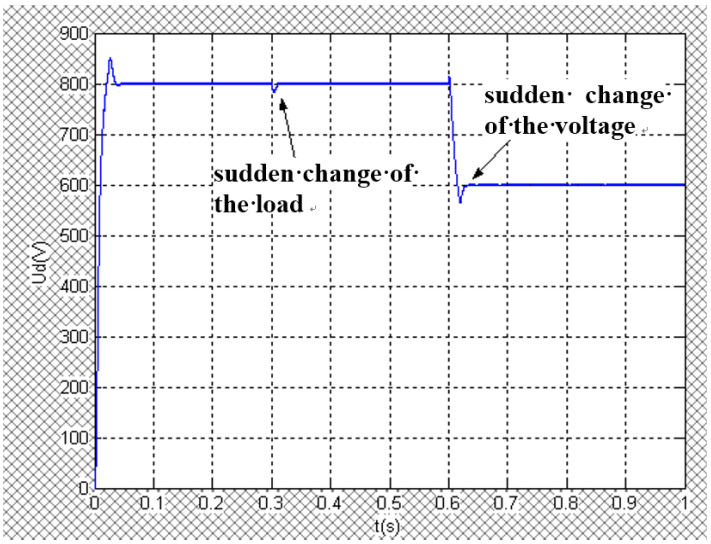

Fig. 3: Output voltage waveform at DC side of rectifier

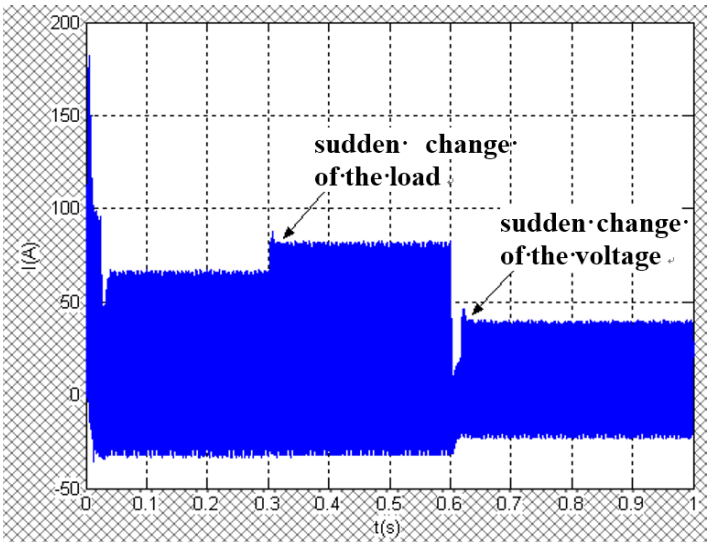

Fig.4: Output current waveform at DC side of rectifier

From Fig. 3, it can be seen that there is a voltage overshoot of about 50V at the DC side of the rectifier during startup; when the load is set to change from 100 Ω to 50 Ω at 0.3s, the DC side output voltage drops by about 15V, and the disturbance recovery time is 12ms. when the given voltage at DC side changes, there is a 30ms disturbance in the waveform. It can be seen from Fig. 4 that the average DC current increases when the load changes and decreases when the given voltage decreases.

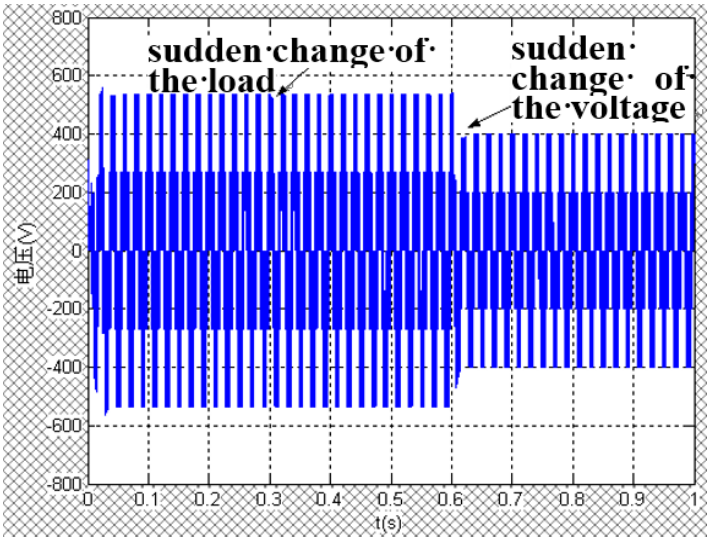

Fig.5: Waveform of phase to ground voltage at AC side of rectifier

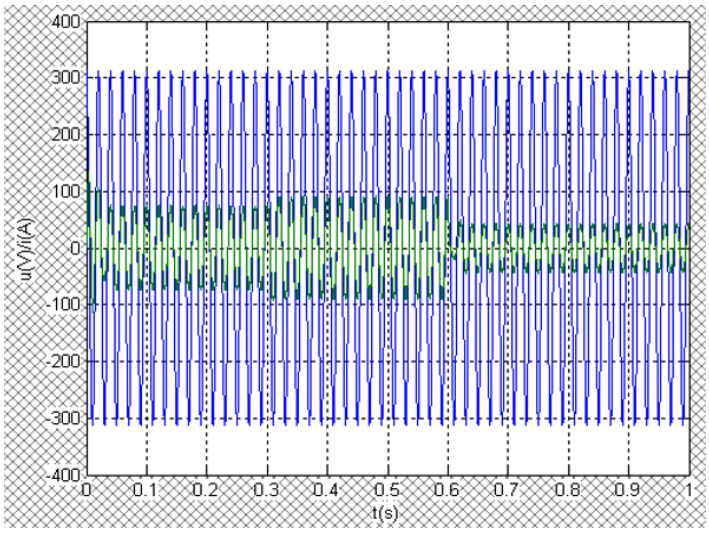

Fig.6: Waveform of input current and voltage of AC power supply

From Fig. 5, it can be seen that the DC output changes little when the load changes suddenly. It can be seen from Fig. 6 that the AC side voltage and current are almost in phase and sine wave regardless of the given change of load or DC voltage. When disturbance occurs, the current waveform returns to normal sine wave after about 5ms regulation. From the simulation results, it can be seen that whether the load size changes or the DC side current changes, it can reflect the effectiveness of predictive current control, reduce the output disturbance, and the system quickly returns to normal operation.

6.2 Experiment

In order to verify the theoretical analysis of PWM rectifier model, discrete-time model and predictive current control strategy, the main circuit, control circuit and protection circuit are built and tested on the basis of simulation.

(1) The main circuit parameters of PWM rectifier open-loop experiment are as follows, AC power line voltage is 220V, inductance L=6mH, resistance R= 0.5Ω, direct side filter capacitance is 1360 μF, load resistance R_L=20Ω, and switching frequency is set at 6kHz.Set the initial phase ξ=30° and modulation M=0.8. The experimental waveform is shown in Fig. 7. The experimental results are U_{DC}=460V, φ= 6°, which is basically consistent with the theoretical calculation results.

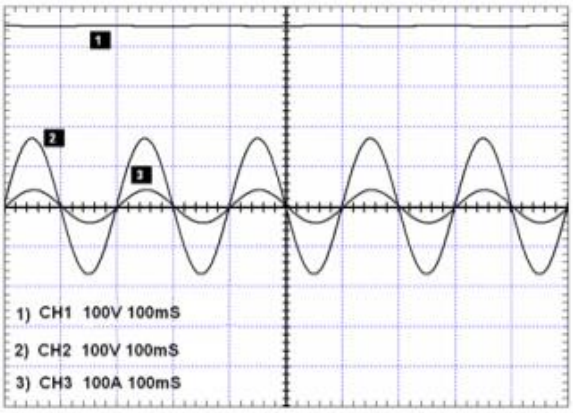

Fig.7: Output waveform of rectifier when ξ=30 ° and M=0.8

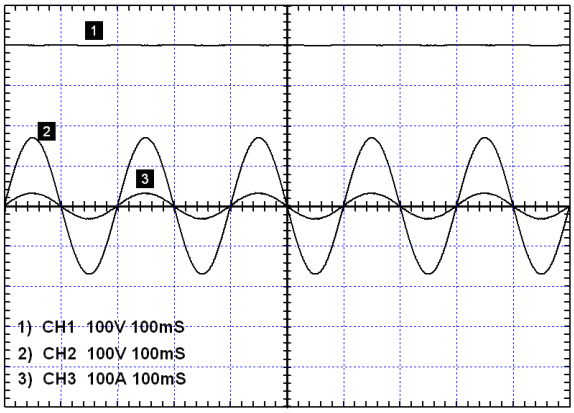

Fig. 8: Output waveform of rectifier when φ = 0°

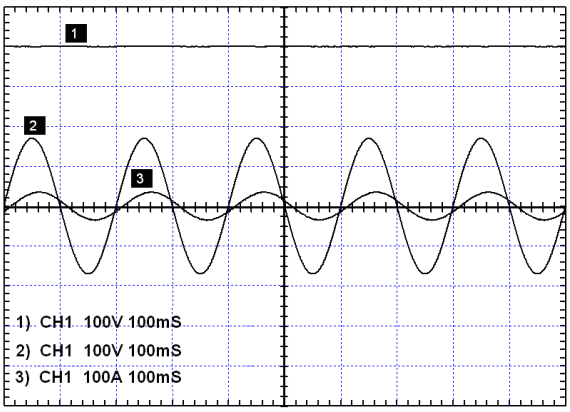

Fig.9: Output waveform of rectifier when φ = 25°

(2) The main circuit parameters of PWM rectifier closed-loop experiment are the same as those of open-loop experiment. (1) Set U_{DC}*=400V, φ^*=0ºand the experimental waveform is shown in Fig. 8. The experimental results show that U_{DC}= 400V, φ^*=0º. (2) Set U_{DC}* = 400V, φ^*=25º (lag), and the experimental

waveform is shown in Fig. 9. The experimental results show that U_{DC} = 400V, φ=24.5º.

From the experimental waveforms, we can see that the DC voltage output is basically stable, the phase of phase a current waveform is basically consistent with the voltage waveform phase, the system power factor is about 1, and the steady-state performance of the system meets the requirements, which indicates that predictive current control can achieve the desired goal.

(3) Battery charging test. After startup, the closing indicator light is on (green), and the constant current indicator is on. When the constant current charging reaches the set voltage value, the pulse depolarization charging is started to eliminate the over-voltage phenomenon caused by constant current charging, so as to make time and technical preparation for automatic switching to constant voltage charging. At this time, the control system continuously identifies the set value of depolarization voltage to constant voltage, and automatically switches to constant voltage charging after confirmation. When the charging current is constant with the voltage, the current will be gradually reduced to activate the deep layer of the plate, so as to ensure that the battery will not be overcharged, improve the ability of the battery to discharge continuously and ensure the safety of charging. The normal charging time is 8-12 hours, and manual shutdown is required after full charging. The voltage withstand test is conducted according to the test voltage values in Tab. 1 for 5 minutes between the charged parts insulated from each other and between the charged parts and the shell, and there is no breakdown or flashover phenomenon.

Table 1

Rated operating voltage and test voltage

Rated operating Voltage U(V)	U≤60	60<U≤300	300<U≤660	660<U≤1140
Test voltage U(V)	380	660	1140	2000

7. Conclusion

In this paper, the rectifier of mine electric locomotive charger is studied. The active front-end PWM rectifier is used as AC-DC link for power supply. The vector control model of PWM rectifier is studied in detail. The predictive current control strategy is adopted based on the active front-end rectifier. The experimental results show that the control system designed in this paper can fully meet the requirements of mine electric locomotive charging device. Through the trial use of the battery, it can basically meet the requirements of stable charging, fast response, stable output and wide adjustable range (the charging device can work normally under the condition of ± 5% grid voltage fluctuation and can ensure constant current operation under 70-100% rated output current, and its constant current accuracy is not less than ± 5%). Thus, the system has good

security.

Acknowledgement

This work was supported in part by teaching innovation team of Mechatronics Technology Education Teachers (No. 2019cxtd110), Key Projects of Natural Science Research in Colleges and Universities of Anhui Province No. KJ2021A1600, KJ2021A1599).

REFERENCES

[1] *Wang, Y.Q., Zhu, Y.C., Zhang, X.G., Tian, B., Wang, K.W., Liang, J.*, Anti-disturbance Sliding Mode Based Deadbeat Direct Torque Control for PMSM Speed Regulation System. IEEE Transactions on Transportation Electrification, vol.7, no.4, pp.2705-2714, 2021. DOI: 10.1109/TTE.2021.3083074.

[2] *Shao, B., Zhu,Z.Q., Feng,J.H., Guo, S.Y., Li, Y.F., Liao, W.*, Compensation of Selective Current Harmonics for Switching-Table-Based Direct Torque Control of Dual Three-Phase PMSM Drives. IEEE Transactions on Industry Applications, vol.57, no.3, pp.2505-2515, 2021. DOI: 10.1109/TIA.2021.3059190.

[3] *Yu, Z.X., Kong, W.B., Qu, R.H., Li, Z.M., Li, D.W.*, Dual-Inverter PWM Scheme for dc-biased Vernier Reluctance Machines with Reduced Switching Frequency Capable of Zero Sequence Current Regulation. IEEE Transactions on Industrial Electronics, vol.69, no.2, pp.1276-1287, 2022. DOI: 10.1109/TIE.2021.3055165.

[4] *Ali, A.I.M., Takeshita, T., Sayed, M.A.*, Three-Phase PWM Inverter for Isolated Grid-Connected Renewable Energy Applications. Energies, vol.14, no.12, pp. 3701, 2021. DOI: 10.3390/en14123701.

[5] *Chen, Q.H., Lin, T.L., Ren, H.L.*, Direct torque control of a permanent magnet synchronous machine for hybrid hydraulic excavator. IET Electric Power Applications, vol.13, no.2, pp.222-228, 2019. DOI: 10.1049/iet-epa.2018.5180.

[6] *Ekanayake, S., Dutta, R., Rahman, M.F., Bui, M.X.*, Performances of a Fractional-Slot Concentrated-Winding Permanent Magnet Synchronous Machine under Position Sensorless Control in Deep Flux-Weakening Region. IEEE Transactions on Industry Applications, vol.55, no.6, pp.5938-5946, 2019. DOI: 10.1109/TIA.2019.2931269.

[7] *Chen, Q.H., Lin, T.L., Ren, H.L.*, A Novel Control Strategy for an Interior Permanent Magnet Synchronous Machine of a Hybrid Hydraulic Excavator. IEEE Access, vol.6, pp.3685-3693, 2018. DOI: 10.1109/ACCESS.2017.2787732.

[8] *Zhang, K., Fan, M.D., Yang, Y., Zhu, Z.K., Garcia, C., Rodriguez, J.*, Field Enhancing Model Predictive Direct Torque Control of Permanent Magnet Synchronous Machine. IEEE Transactions on Energy Conversion, vol.36, no.4, pp.2924-2933, 2021. DOI: 10.1109/TEC.2021.3070339.

[9] *Rodriguez, J.R., Dixon, J.W., Espinoza, J.R., Pontt, J., Lezana, P.*, PWM regenerative rectifiers: state of the art. IEEE Transactions on Industrial Electronics, vol.52, no.1, pp.5-22, 2005. DOI: 10.1109/TIE.2004.841149.

[10] *Le, V.T., Lee, H.H.*, An Enhanced Model-Free Predictive Control to Eliminate Stagnant Current Variation Update for PWM Rectifiers. IEEE Journal of Emerging and Selected Topics in Power Electronics, vol.9, no.6, pp.6804-6816, 2021. DOI: 10.1109/JESTPE.2021.3058737.

[11] *Malinowski, M., Kazmierkowski, M.P., Trzynadlowski, A.M.,* A comparative study of control techniques for PWM rectifiers in AC adjustable speed drives. IEEE Transactions on Power Electronics, vol.18, no.6, pp.1390-1396, 2003. DOI: 10.1109/TPEL.2003.818871.

[12] *Ming, L., Ding, W.L., Yin, C.Q., Xin, Z., Loh, P.C.,* A Generic Two-Stage Carried-Based PWM Scheme with Adjustable Switching Patterns for Current Source Converter. IEEE Journal of Emerging and Selected Topics in Power Electronics, vol.9, no.5, pp.6033-6048, 2021. DOI: 10.1109/JESTPE.2021.3059709.

[13] *Marquez Alcaide, A., Monopoli, V.G., Wang, X.C., Leon, J.I., Buticchi, G., Vazquez, S., Liserre, M., Franquelo, L.G.,* Common-Mode Voltage Harmonic Reduction in Variable Speed Drives Applying a Variable-Angle Carrier Phase-Displacement PWM Method. Energies, vol.14, no.10, pp. 2929, 2021. DOI: 10.3390/en14102929.

[14] *Ahmed, H.F., EI Moursi, M.S., Zahawi, B., AI Hosani, K.,* A High-Frequency Isolated Multilevel Cascaded-Type Bipolar Direct PWM AC-AC Converter for Utility Voltage Compensation. IEEE Transactions on Industry Applications, vol.57, no.3, pp.3188-3201, 2021. DOI: 10.1109/TIA.2020.3021371.

[15] *Zhang L., Li L.,* Analysis of Reactive Power Compensation Strategy for Mine Hoist Based on Instantaneous Power Theory. Coal Mine Machinery, vol.38, no.1, pp.40-42, 2017. DOI: 10.13436/j.mkjx.201701015.

[16] *Morais, V.A., Afonso, J.L., Carvalho, A.S., Martins, A.P.,* New Reactive Power Compensation Strategies for Railway Infrastructure Capacity Increasing. Energies, vol.13, no.17, pp. 4379, 2020. DOI:10.3390/en13174379.

[17] *Ikeda, F., Nishikawa, K., Okamoto, Y., Yamada, H., Tanaka, T., Okamoto, M.,* Simple Power Quality Compensation with Bidirectional Battery Charger for Electric Vehicles in Single-Phase Three-Wire Distribution Feeders. Energies, vol.13, no.11, pp. 2894, 2020. DOI: 10.3390/en13112894.

[18] *Zhang L., Li L.,* Analysis of reactive power control strategy of mine hoist based on generalized current minimization theory. Coal mine machinery, vol.39, no.8, pp.76-77, 2018. DOI: 10.13436/j.mkjx.20180827.

[19] *Huang, Y., Li, C.H., Liu T.,* Research on coordinated reactive power control strategy of hybrid-HVDC. The Journal of Engineering, vol. 2019, no.16, pp. 3349-3353, 2019. DOI: 10.1049/joe.2018.8857.

[20] *Tseng, C.W., Liu, J.H., Pan, C.T., Chu C.C.,* Dual PWM Control for High Step-Down DC-DC Converters. IEEE Transactions on Industry Applications, vol. 56, no. 4, pp. 4272-4287, 2020. DOI: 10.1109/TIA.2020.2993220.

[21] *Shan, Y.H., Hu, J.F., Chan, K.W, Fu, Q., Guerrero, J.M.,* Model Predictive Control of Bidirectional DC-DC Converters and AC/DC Interlinking Converters-A New Control Method for PV-Wind-Battery Microgrids. IEEE Transactions on Sustainable Energy, vol. 10, no. 4, pp. 1823-1833, 2019. DOI: 10.1109/TSTE.2018.2873390.

[22] *Dekka, A., Wu, B., Yaramasu, V., Fuentes, R. L., & Zargari, N. R.,* Model Predictive Control of High-Power Modular Multilevel Converters — An Overview. IEEE Journal of Emerging and Selected Topics in Power Electronics, vol. 7, no. 1, pp. 168-183, 2019. DOI: 10.1109/JESTPE.2018.2880137.